AJNR

Characterizing the Mesencephalon Using Susceptibility-Weighted Imaging

E.S. Manova, C.A. Habib, A.S. Boikov, M. Ayaz, A. Khan, W.M. Kirsch, D.K. Kido and E.M. Haacke

AJNR Am J Neuroradiol 2009, 30 (3) 569-574
doi: https://doi.org/10.3174/ajnr.A1401
http://www.ajnr.org/content/30/3/569

This information is current as of August 15, 2025.

ORIGINAL RESEARCH

Characterizing the Mesencephalon Using Susceptibility-Weighted Imaging

E.S. Manova
C.A. Habib
A.S. Boikov
M. Ayaz
A. Khan
W.M. Kirsch
D.K. Kido
E.M. Haacke

BACKGROUND AND PURPOSE: The mesencephalon is involved in a number of human neurodegenerative disorders and has been typically imaged with T1-, T2- and T2*-weighted methods. Our aim was to collect high-contrast susceptibility-weighted imaging (SWI) data to differentiate among and within the basic mesencephalic structures: namely, the red nucleus, substantia nigra, and crus cerebri.

MATERIALS AND METHODS: High-resolution SWI, 3D T1-weighted, and T2-weighted data were collected to study contrast in the mesencephalon at 1.5T and 4T. Contrast between structures was calculated for SWI high-pass (HP)-filtered-phase, T1 gradient-echo, and spin-echo T2-weighted data.

RESULTS: SWI HP-filtered-phase data revealed similar contrast for the red nucleus and substantia nigra when compared with T2-weighted imaging. However, SWI was able to show structures within the red nucleus, substantia nigra, and medial geniculate body that were invisible on T2-weighted imaging. T1-weighted imaging, on the other hand, did not reveal measurable contrast for any of the structures of interest. SWI HP-filtered-phase data at 4T agreed well with india ink–stained cadaver brain studies, which appear to correlate with capillary density.

CONCLUSIONS: With SWI, it is possible to create better anatomic images of the mesencephalon, with improved contrast compared with conventional T1- or T2-weighted sequences.

In recent years, imaging of neurodegenerative disorders like Alzheimer, Parkinson, and Huntington diseases has attracted much attention. Most of the pathologic landmarks of these diseases have been found in parts of the brain stem, especially in the mesencephalon. The substantia nigra, which is the primary source of dopamine synthesis and whose pathways are known to involve iron,[1] is affected in a number of diseases. Its atrophy and/or altered functionality could lead to a disruption of dopamine balance in the brain and may lead to motor and/or cognitive deficits. Two other structures involved in coordinating motor function are the crus cerebri (located lateral to the substantia nigra) and the red nucleus, which has connections to the cerebellum and the spinal cord via a number of key motor tracts. The progression of Alzheimer, Parkinson, and Huntington diseases has been thought to be associated with an increase in iron content in the red nucleus and substantia nigra.[2] Therefore, the ability to differentiate mesencephalic structures should be helpful in visualizing specific damage to these structures and establishing better diagnoses for neurodegenerative diseases.[1-5]

To date, T1-, T2-, and T2*-weighted MR imaging methods have been used to image the mesencephalon.[6] Generally, the workhorse in anatomic measurements has been 3D T1-weighted gradient-echo imaging. This is often performed with a magnetization-prepared rapid acquisition of gradient echo (MPRAGE) approach that uses an inversion pulse followed by the section-encoding gradients and then loops over the phase-encoding gradients.[7] Alongside MPRAGE, a short-TR low flip angle gradient-echo fast low-angle shot sequence with radiofrequency spoiling can be used for T1 contrast.[8] As an example of applied research in imaging the mesencephalon, Shibata et al[9] used T1-weighted imaging to investigate changes in neuromelanin levels in the lower tegmentum. Unfortunately, such T1-based sequences provide rather poor information about upper mesencephalic structures where high vascularization is present[1] and where accurate differentiation of gray matter structures is needed. T2-weighted imaging shows the substantia nigra and the red nucleus quite well but does not distinguish their substructures (such as the pars reticulata and pars compacta of the substantia nigra or the capsule and interior structures of the red nucleus). Today, at 3T and 4T, resolution can be pushed easily to $0.5 \times 0.5 \times 2$ mm^3. This level of resolution should allow good 3D imaging of the mesencephalon, given that the structures of interest are only about 1 cm thick and require thin sections to be evaluated in detail.

Recently, a method called susceptibility-weighted imaging (SWI) has been developed to enhance contrast in T2*-weighted imaging.[10,11] It is performed by using a fully flow-compensated gradient-echo imaging method to pick up extra information from local susceptibility variations in tissue via the phase image (in the past, phase was usually discarded as not being useful clinically). Due to the fact that the phase signal intensity is sensitive to local field-change effects, phase data are used as a new source of contrast. When the MR imaging data are collected, there are both real and imaginary components. These are then rearranged to create magnitude and phase images. The phase images contain information about local static field variations, geometry-induced field variations, and the local tissue susceptibility of interest. The first 2 components tend to have low spatial frequency and can be mostly eliminated by applying a high-pass (HP) filter. The resulting HP-filtered-phase images can be considered to be a reasonable representation of the local tissue susceptibility.[12]

Susceptibility changes can be caused by deoxygenated

Received April 8, 2008; accepted after revision October 3.

From the Department of Biomedical Engineering (E.S.M., C.A.H., M.A., A.K., E.M.H.), Wayne State University, Detroit, Mich; The MRI Institute for Biomedical Research (C.A.H., A.S.B., M.A., E.M.H.), Detroit, Mich; and Departments of Radiology (D.K.K., E.M.H.) and Neurosurgery (W.M.K.), Loma Linda University, Loma Linda, Calif.

This work was supported in part by the National Institutes of Health Grant AG20948 and by the State of Michigan Grant 085P5200251.

Please address correspondence to E. Mark Haacke, PhD, The MRI Institute for Biomedical Research, 440 E Ferry St, Unit 2, Detroit, MI 48202; e-mail: nmrimaging@aol.com

Indicates open access to non-subscribers at www.ajnr.org

DOI 10.3174/ajnr.A1401

blood (due to the paramagnetic nature of deoxyhemoglobin), brain iron (in the form of ferritin or hemosiderin proteins), or calcium (which is diamagnetic). The SWI HP-filtered-phase images are themselves of anatomic interest and can be used to measure the putative nonheme iron content in the basal ganglia and in other areas of the brain.[12] The SWI HP-filtered-phase images can also be modified to produce a phase mask that is then multiplied into the magnitude images to create a set of SWI magnitude images.[10,11] These new images now carry unique information from the phase and provide improved contrast between veins, arteries, and surrounding tissue.

Although SWI has been used to show individual images of the mesencephalon previously,[11-15] no one, to our knowledge, has yet performed a systematic and quantitative analysis of the contrast between the different structures of the midbrain. In the present work, we quantified contrast between and within structures in the human mesencephalon at 1.5T and 4T using SWI. Specifically, the following structures will be shown on SWI HP-filtered-phase images: the red nucleus and its vascular subcomponents, the capsule of the red nucleus, the substantia nigra pars compacta, the substantia nigra pars reticulata, the crus cerebri, the medial geniculate body, the lateral geniculate body, the subthalamic nucleus, and the fascicula nigrale (the pallidal-nigral pathway). The contrast of these structures, provided by SWI HP-filtered-phase images, will be shown to correlate with the contrast defined by the vascular content in the mesencephalon, highlighted by the india ink staining of cadaver brains in Duvernoy's work.[16] High-resolution examples covering the entire mesencephalon (5 sections, each 2 mm thick) will be shown at both 1.5T and 4T.

Materials and Methods

Five volunteers (23–27 years of age for SWI; 36–56 years of age for T1 and T2) were imaged at 1.5T (Sonata; Siemens, Erlangen, Germany), and another 5 volunteers (23–27 years of age for SWI; 29–45 years of age for T1 and T2) were imaged at 4T (MedSpec; Bruker/Siemens, Ettlingen, Germany). Institutional review board approval was obtained, and all participants signed the appropriate consent forms. All images were collected in a predominantly axial orientation following the anterior/posterior commissure line. Detailed imaging protocols are given below.

1.5T Imaging Protocol

A segmented echo-planar imaging sequence (5 echoes) was used for the SWI scans. The sequence was performed with a resolution of $0.5 \times 0.5 \times 2$ mm^3, 64 sections, TR = 71 ms, TE = 40 ms, bandwidth (BW) = 130 Hz/pixel, flip angle (FA) = 20°, a matrix size of 512×512, and an acquisition time of 8 minutes 57 seconds. The 3D T1-weighted images were obtained with a resolution of $0.5 \times 0.5 \times 2$ mm^3, 64 sections (with a parallel imaging factor of 2), TR = 20 ms, TE = 5.58 ms, BW = 130 Hz/pixel, FA = 25°, a matrix size of 512×512, and an acquisition time of 4 minutes 11 seconds. The T2 data were obtained with a resolution of $0.5 \times 0.5 \times 4$ mm^3, 25 sections, TR = 5230 ms, TE = 106 ms, FA = 160°, BW = 130 Hz/pixel, a matrix size of 512×384, and an acquisition time of 4 minutes 47 seconds.

Imaging Protocol at 4T

A fully flow-compensated gradient-echo sequence was used for the SWI scans. The sequence was performed with a resolution of $0.5 \times 0.5 \times 2$ mm^3, 64 sections, TR = 24 ms, TE = 15 ms, BW = 80 Hz/pixel, FA = 12°, a matrix size of 512×512, and an acquisition time of 12 minutes 52 seconds. The 3D T1-weighted images were obtained with a resolution of $0.5 \times 0.5 \times 2$ mm^3, 64 sections (with a parallel imaging factor of 2), TR = 20 ms, TE = 5.58 ms, BW = 130 Hz/pixel, FA = 25°, a matrix size of 512×512, and an acquisition time of 4 minutes 47 seconds. The T2 data were obtained with a resolution of $0.8 \times 0.8 \times 3$ mm^3, 36 sections, TR = 4950 ms, TE = 72 ms, FA = 150°, BW = 120 Hz/pixel, a matrix size of 320×240, and an acquisition time of 4 minutes 53 seconds.

Evaluating the Data

The data were processed with in-house Visual C++-based software, Signal Processing in NMR (SPIN, Detroit, Mich). SWI data were processed by using a 64×64 HP filter to create a filtered-phase image. Window level setting adjustments were made to view the best image contrast. In measuring contrast, we measured the signal intensity for a given structure from a 100- to 200-pixel region of interest drawn within the structure of interest. For SWI phase and all conventional sequences, contrast-to-noise ratios (CNRs) were calculated as the signal-intensity difference between 2 structures (S_a, S_b), divided by the noise (σ), or $(S_a - S_b) / \sigma$. The noise was calculated as 0.8 times the mean of a 100- to 200-pixel region of interest outside the head and away from phase-encoding artifacts (a region where only noise was present).

Because the structures measured were bilateral, the CNR for a given structure was measured from the region of interest having the best apparent contrast. Where the appropriate contrast was visible, we calculated the CNR between the following areas: the red nucleus and the intermediate area that separates the red nucleus from the substantia nigra, the red nucleus and its capsule, the capsule of the red nucleus and the intermediate area, the substantia nigra and the intermediate area, the substantia nigra and the crus cerebri, the substantia nigra pars compacta and the substantia nigra pars reticulata, the substantia nigra pars compacta and the intermediate area, the substantia nigra pars reticulata and the crus cerebri, the lateral and central aspects of the medial geniculate body, and the central aspect of the medial geniculate body and the intermediate area. Background noise was also evaluated outside the image and compared with the SD seen inside the region of interest. Each subject dataset was carefully scrutinized to find the sections associated with the mesencephalic structures of interest. The MR imaging results were compared with the measurements of mesencephalic capillary density in cadaver brains by Duvernoy,[16] who (by using 3-mm-thick sections) performed india ink staining and 5% gelatin injections to highlight anatomic differences.

Results

The area reviewed in the mesencephalon is shown in Fig 1. A comparison between T1, T2, and SWI contrast, alongside Duvernoy's india ink–stained results,[16] is shown in Fig 2. Overall, there is little apparent contrast in the T1-weighted images, whereas the T2-weighted images show good contrast for the red nucleus and substantia nigra. The SWI images, however, appear to show good contrast with details of the internal structures visible for the red nucleus, the substantia nigra, the crus cerebri, and the medial geniculate body (Fig 3). On the SWI HP-filtered-phase images, we see the red nucleus broken up into a highly vascularized portion and a less-vascularized portion.

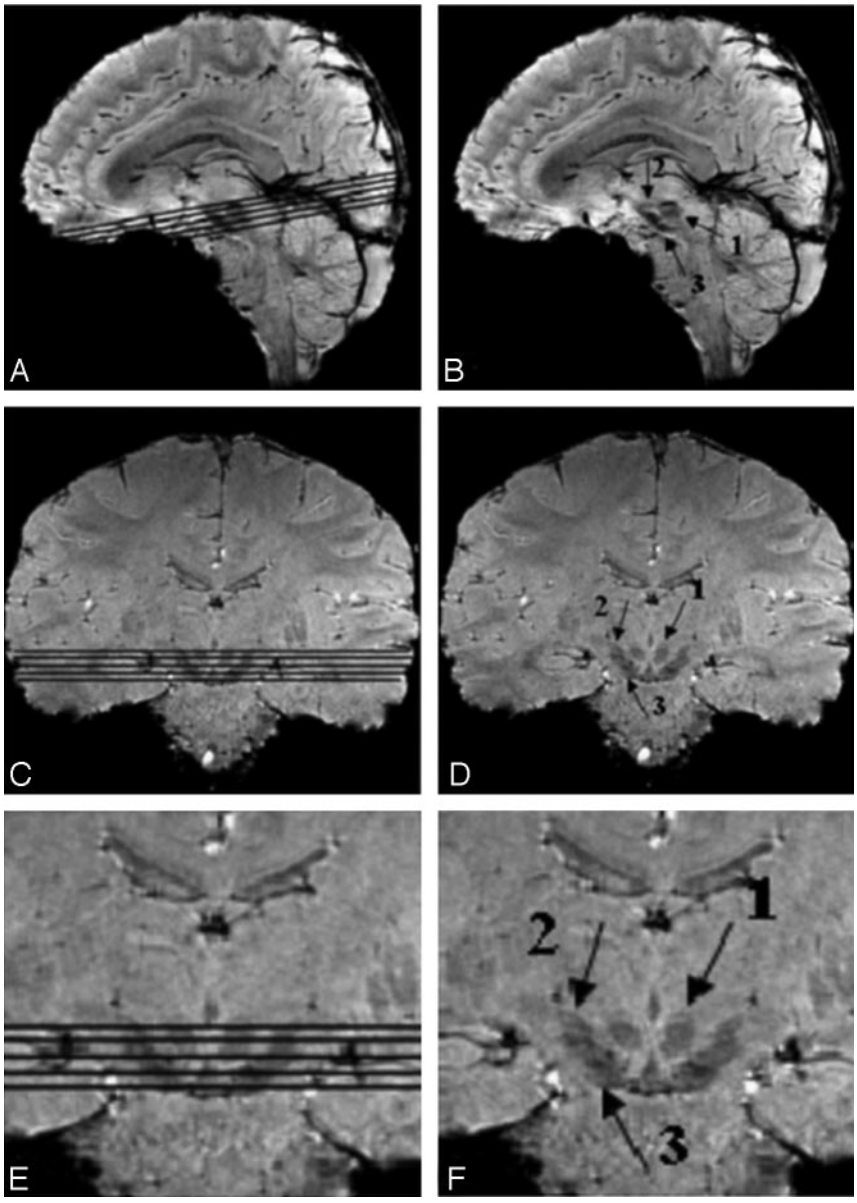

Fig 1. The midbrain as a region-of-interest on 4T SWI magnitude images shown in sagittal and coronal sections, with and without section locators. Arrows 1, 2, and 3 point to the red nucleus, the subthalamic nucleus, and the substantia nigra, respectively.

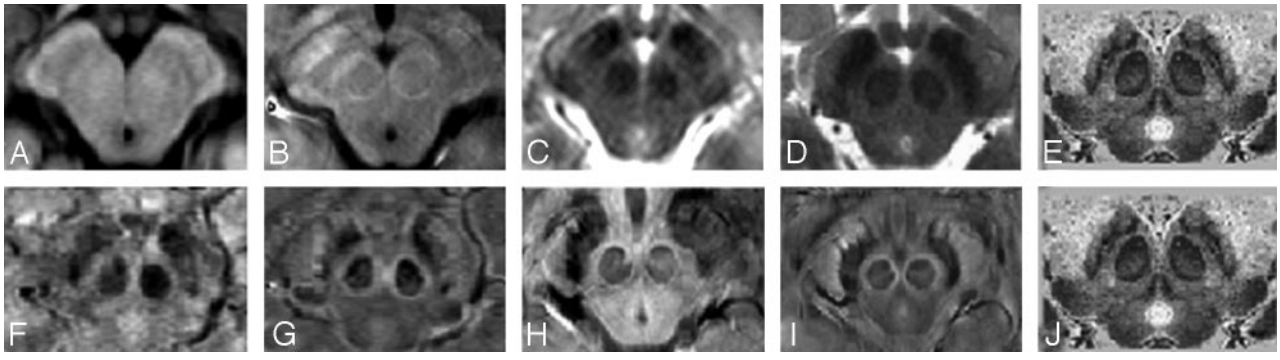

Fig 2. A comparison of 1 region of the mesencephalon for different sequences and field strengths with Duvernoy's stained cadaver brain results.[16] *A*, T1 at 1.5T; *B*, T1 at 4T; *C*, T2 at 1.5T; *D*, T2 at 4T; *E*, Duvernoy's india ink-stained image; *F*, SWI magnitude at 1.5T; *G*, SWI HP-filtered phase at 1.5T; *H*, SWI magnitude at 4T; *I*, SWI HP-filtered phase at 4T; *J*, Duvernoy's india ink-stained image. Images *E* and *J* reprinted with permission from Duvernoy HM. *Human Brain Stem Vessels*. 2nd ed. Berlin, Germany: Springer-Verlag; 1999;206–13.

The images from Duvernoy[16] show the horseshoe effect of the vascularized red nucleus, and this is well mimicked in the SWI results (Fig 4*C*, -*D*; arrow 4a). Also, the connecting tissue from the substantia nigra is seen to course laterally through the

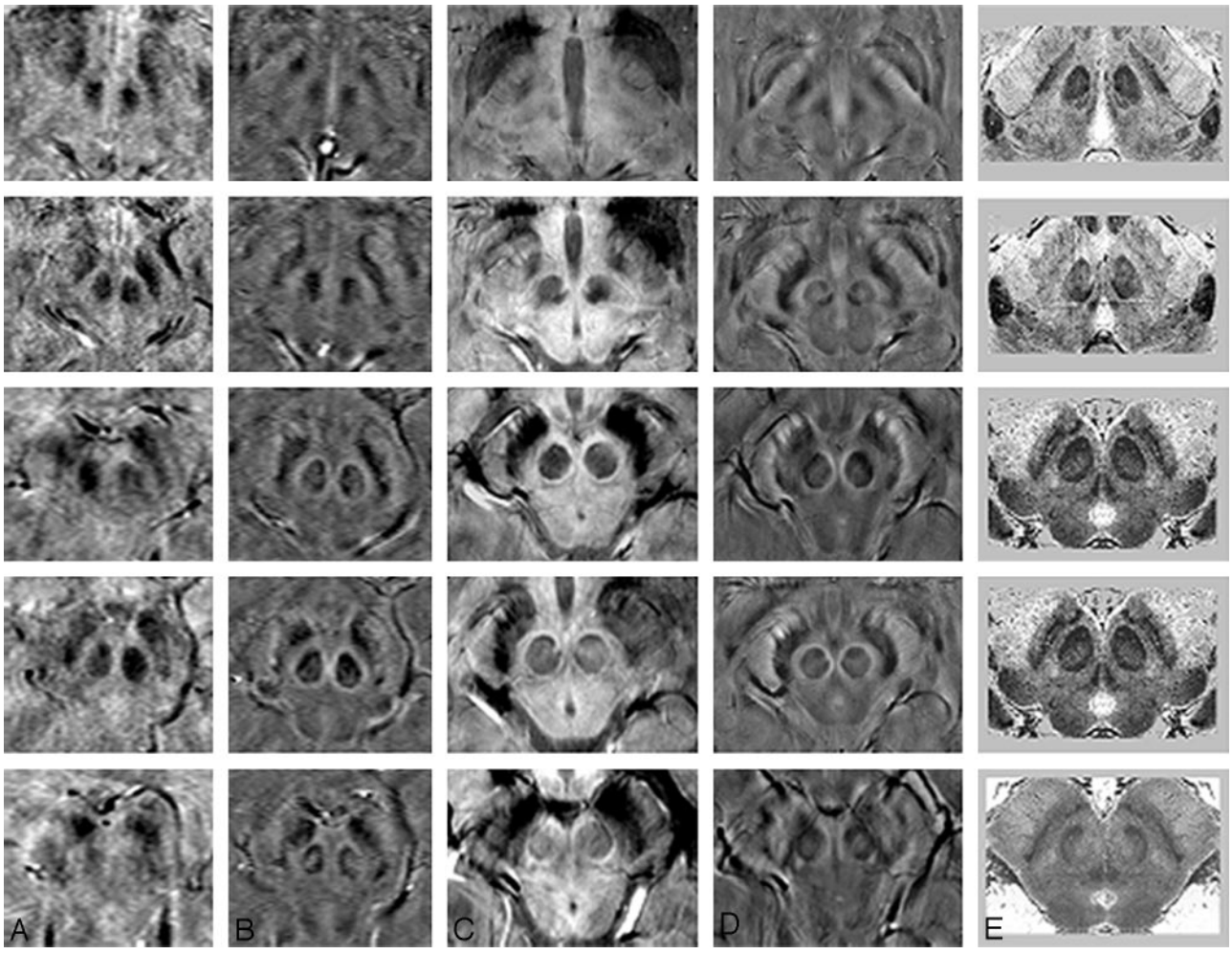

Fig 3. A comparison of adjacent sections in SWI magnitude and HP-filtered-phase images at 1.5T and 4T with Duvernoy's india ink-stained results.[16] *A,* Magnitude SWI at 1.5T; *B,* HP-filtered phase at 1.5T; *C,* Magnitude SWI at 4T; *D,* HP-filtered phase at 4T; *E,* Duvernoy's results. Only 3 unique images from Duvernoy are shown here because his section thickness is 3 mm. The third and fourth images from the top are identical. Images in column *E* reprinted with permission from Duvernoy HM. *Human Brain Stem Vessels.* 2nd ed. Berlin, Germany: Springer-Verlag; 1999;206–13.

crus cerebri (Fig 4*C*, -*D*; arrow 1). The substantia nigra can occasionally be seen as having 2 parts: the pars reticulata (the lateral portion, containing more iron; Fig 4; arrow 2a) and the pars compacta (the medial portion, containing slightly less iron; Fig 4; arrow 2b). Similar to the behavior seen in the red nucleus, the dark, more vascularized region in the lateral aspect of the medial geniculate body is shown in SWI (Fig 4; arrow 6). Finally, the pallidal-nigral pathway (the fascicula nigrale)—which may transport iron between the substantia nigra and globus pallidus—is also seen (Fig 4*B*−*D*; arrow 5). Much of the anatomy of these structures changes with each 2-mm-thick section, and many details would not be visible with thicker sections.

In terms of capillary density, the patterns shown in Duvernoy's work[16] appear to be duplicated in the SWI phase images. In addition to the differentiation displayed within the substantia nigra, the red nucleus is seen to contain 2 regions: a highly vascularized horseshoe area and a brighter central region (Fig 4*C*, -*D*; arrows a and b). In general, the local decrease in phase correlates with the darkened patterns of vascularization in Duvernoy's work.

In terms of quantitative tissue differentiation, we have found that SWI HP-filtered-phase provides good contrast, especially when considering all the components of the mesencephalon. CNR measurements are provided in Table 1 for 1.5T and Table 2 for 4T. The effect of an improved signal intensity–to-noise ratio at high field and reduced T2 is evident in the images wherever iron content is high. In SWI, the CNR generally increases from 1.5T to 4T, but this increase is dependent on the structure of interest. In some cases (eg, in the medial geniculate body), the CNR increases by a factor of 3 from 1.5T to 4T. In other cases, there is only a 25% increase in CNR (eg, in the red nucleus). Although T2-weighted imaging appears to show quite good contrast for the substantia nigra at both field strengths, with SDs taken into account, these mean CNR values are similar for both techniques. However, HP-filtered-phase SWI shows statistically better contrast between the intermediate area and the substantia nigra at 4T than does T2 (8.75 ± 1.67 for SWI versus 4.53 ± 0.48 for T2). This is also the case for contrast between the intermediate area and the red nucleus at 4T (6.98 ± 2.60 for SWI versus 3.36 ± 0.77 for T2). SWI HP-filtered-phase reveals measurable contrast for structures for which T2 does not: specifically, the capsule of the red nucleus, the pars compacta and pars reticulata of the substan-

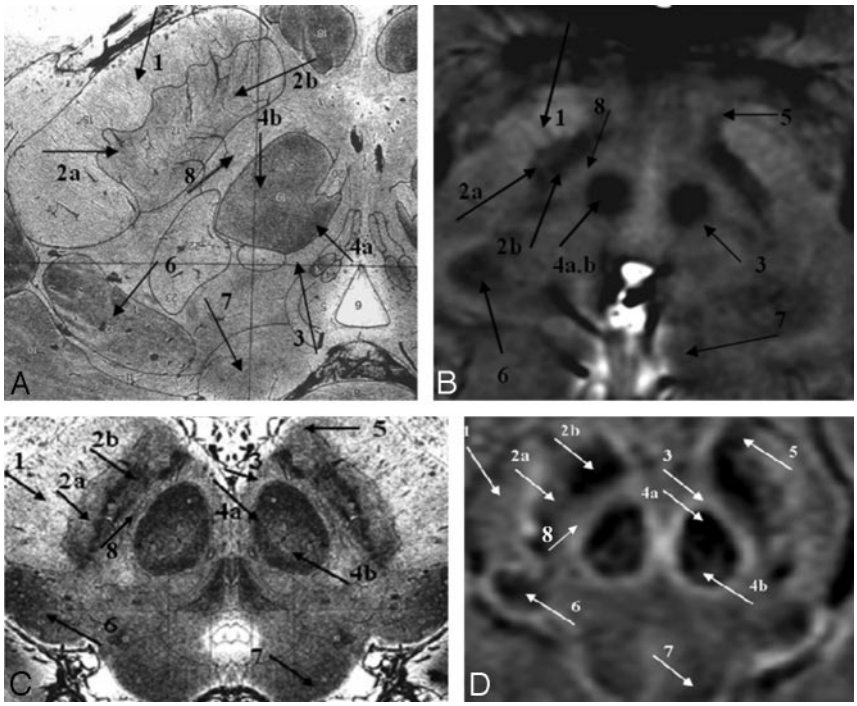

Fig 4. A comparison of SWI HP-filtered-phase images (*B* and *D*) with Duvernoy's india ink–stained results (*A* and *C*).[16] Anterior (*A* and *B*) and posterior (*C* and *D*) mesencephalic structures are indicated. Arrow 1 indicates the crus cerebri; 2a, substantia nigra, pars reticulata; 2b, substantia nigra, pars compacta; 3, capsule of the red nucleus; 4a, red nucleus (vascularized region); 4b, red nucleus (nonvascularized region); 5, fascicula nigrale; 6, medial geniculate body; 7, superior colliculus; 8, intermediate area. Images *A* and *C* reprinted with permission from Duvernoy HM. *Human Brain Stem Vessels.* 2nd ed. Berlin, Germany: Springer-Verlag; 1999;206–13.

Table 1: 1.5T CNR measurements*

	Red Nucleus CNR			Substantia Nigra CNR			Medial Geniculate CNR	
Sequence	IA/RN	IA/RN capsule	RN/RN capsule	IA/SNc	CC/SNr	SNc/SNr	CMG/LMG	CMG/IA
T2 tse	4.13	–	–	6.19†	4.97†	–	–	–
T2 tse SD	1.23	–	–	1.44†	1.48†	–	–	–
SWI	5.97	1.43	4.54	5.58	2.84	3.74	1.38	0.45
SWI SD	1.78	0.73	1.62	0.6	0.75	1.46	1.47	0.35

RN indicates red nucleus; SNc, substantia nigra, pars compacta; SNr, substantia nigra, pars reticulata; IA, intermediate area between the RN and SN; CC, crus cerebri; LMG, lateral aspect of the medial geniculate body; CMG, central aspect of medial geniculate body; tse, turbo spin-echo; CNR, contrast-to-noise ratio.
* The first row for each sequence represents the mean in a given region of interest and the second row represents the SD in the same region of interest. HP-filtered-phase data were used for SWI CNR measurements; no contrast for the given regions of interest was observed in the gradient-echo T1 data. Empty data boxes show that CNRs between certain structures could not be calculated because the structures could not be detected.
† Because SNc and SNr were not separable for T2, CNR is recorded here for IA/SN and CC/SN.

Table 2: 4T CNR measurements*

	Red Nucleus CNR			Substantia Nigra CNR			Medial Geniculate CNR	
Sequence	IA/RN	IA/RN capsule	RN/RN capsule	IA/SNc	CC/SNr	SNc/SNr	CMG/LMG	CMG/IA
T2 tse	3.36	–	–	4.53†	6.27†	–	–	–
T2 tse SD	0.77	–	–	0.48†	1.64†	–	–	–
SWI	6.98	1.13	5.85	8.75	5.19	3.56	4.57	1.64
SWI SD	2.60	1.34	2.23	1.67	1.51	1.08	2.49	0.89

* The first row for each sequence represents the mean in a given region of interest and the second row represents the SD in the same region of interest. HP-filtered-phase data were used for SWI CNR measurements; no contrast for the given regions of interest was observed in the gradient-echo T1 data. Empty data boxes show that CNRs between certain structures could not be calculated because the structures could not be detected.
† Because SNc and SNr were not separable for T2, CNR is recorded here for IA/SN and CC/SN.

tia nigra, and the central and lateral aspects of the medial geniculate body.

Discussion

On the basis of the data collected at 1.5T and 4T, we can see that highly vascularized areas, like the vascularized region of the red nucleus (as specified in Duvernoy's work[16]), become more prominent or darker on SWI HP-filtered-phase images at higher field strength (Figs 2 and 3). Thus, the contrast between the red nucleus and the surrounding brain tissue improves with increasing field strength. In fact, we are able to see the capsule of the red nucleus at 4T in the magnitude images for the first time (Figs 2*H* and 3*C*). (SWI HP-filtered-phase images can visualize the capsule at 1.5T, but the magnitude images do not). Although the CNR is often larger than 4:1 (the CNR needed to be able to differentiate clearly 1 structure from another), this was not always the case. The T2 images had thicker sections (4 mm at 1.5T and 3 mm at 4T); hence, their

CNR is overestimated by the ratio of their thicknesses compared with the 2-mm thickness used in the SWI scans. Furthermore, the CNR at 4T is even further overestimated by a factor of 1.6 because of the comparatively lower 0.8-mm resolution (as opposed to 0.5 mm in the SWI scans).

Iron plays a key role in many neurologic processes. It is of great interest in the study of neurodegenerative disease today and remains a topic of high interest in the medical community. SWI offers a way to look at iron content that is different from T1, T2, or T2* maps. The SWI filtered-phase images are a sensitive means not only to visualize the presence of iron but also to quantify it.[12,17,18] The nonheme forms of iron that are likely seen with MR imaging are ferritin and hemosiderin.[1] Ferritin appears to be seen predominantly in the basal ganglia and primary motor cortex. Gray matter has more ferritin than white matter, though there are indications that ferritin is also present in white matter.[12] Iron in transferrin or in glial cells may be nonmagnetic and, therefore, invisible to MR imaging. This may explain why white matter appears to have less iron than gray matter on MR imaging, whereas staining reveals the opposite.[18]

Hypothetically, if we are able to prove that iron causes a reduction in T2 or T2* with increasing magnetic field strength, we would be able to predict that the areas with the higher capillary density would appear darker at high-field strength. An interesting study would be to investigate the relationship between iron and vascular density. Sofic et al[1] and Morris et al[19] showed that large ferritin deposits are associated with the small blood vessels of the basal ganglia. The strong correspondence of SWI phase and high-field magnitude images with Duvernoy's india ink–stained images[16] and the results of Morris et al,[19] therefore, suggest that the nonheme iron visualized in MR imaging in the normal brain is most likely due to ferritin associated with the vascular network. If this hypothesis is verified, these SWI magnitude and filtered-phase images may also prove to be an important means for understanding microvascular effects in neurodegenerative diseases.

In conclusion, the high iron content in the red nucleus and substantia nigra leads to a susceptibility change in the tissue that causes a reduction of the phase in these regions in the SWI filtered-phase images. This phase change can be used either by itself or to create a magnitude SW image. In either case, this property leads to improved contrast in the mesencephalon by using SWI. The improved contrast in the phase images may provide a means by which to monitor changes in the mesencephalon with age or disease state.

References

1. Sofic E, Paulus W, Jellinger K, et al. **Selective increase of iron in substantia nigra zona compacta in parkinsonian brains.** *J Neurochem* 1991;56:978–82
2. Sohmiya M, Tanaka M, Aihara Y, et al. **Structural changes in the midbrain with aging and Parkinson's disease: an MRI study.** *Neurobiol Aging* 2004;25:449–53
3. Semnic R, Svetel M, Dragasevic N, et al. **Magnetic resonance imaging morphometry of the midbrain in patients with Wilson disease.** *J Comput Assist Tomogr* 2005;29:880–83
4. Kim E, Na DG, Kim EY, et al. **MR imaging of metronidazole-induced encephalopathy: lesion distribution and diffusion-weighted imaging findings.** *AJNR Am J Neuroradiol* 2007;28:1652–58. Epub 2007 Sep 20
5. Sohmiya M, Tanaka M, Aihara Y, et al. **Age-related structural changes in the human midbrain: an MR image study.** *Neurobiol Aging* 2001;22:595–601
6. Gelman N, Gorell JM, Barker PB, et al. **MR imaging of human brain at 3.0 T: preliminary report on transverse relaxation rates and relation to estimated iron content.** *Neuroradiology* 1999;210:759–67
7. Mugler JP, Brookeman JR. **Three-dimensional magnetization-prepared rapid gradient-echo imaging (3D MP RAGE).** *Magn Reson Med* 1990;15:152–57
8. Frahm J, Haase A, Matthei D, et al. **FLASH imaging: rapid imaging using low flip angle pulses.** *J Magn Reson Imaging* 1986;67:256–66
9. Shibata E, Sasaki M, Tohyama K, et al. **Neuromelanin magnetic resonance imaging of locus ceruleus and substantia nigra in Parkinson's disease.** *Neuroreport* 2006;17:1215–18
10. Reichenbach JR, Venkatesan R, Schillinger DJ, et al. **Small vessels in the human brain: MR venography with deoxyhemoglobin as an intrinsic contrast agent.** *Radiology* 1997;204:272–77
11. Haacke EM, Xu Y, Cheng YN, et al. **Susceptibility-weighted imaging (SWI).** *Magn Reson Med* 2004;52:612–18
12. Haacke EM, Ayaz M, Khan A, et al. **Establishing a baseline phase behavior in magnetic resonance imaging for determining normal versus abnormal iron content in the brain.** *J Magn Reson Imaging* 2007;26:256–64
13. Abduljalil AM, Schmalbrock P, Novak V, et al. **Enhanced gray and white matter contrast of phase susceptibility-weighted images in ultra-high-field magnetic resonance imaging.** *J Magn Reson Imaging* 2003;18:284–90
14. Rauscher A, Sedlacik J, Barth M, et al. **Magnetic susceptibility-weighted MR phase imaging of the human brain.** *AJNR Am J Neuroradiol* 2005;26:736–42
15. Chakeres DW, Abduljalil AM, Novak P, et al. **Comparison of 1.5 and 8 Tesla high-resolution magnetic resonance imaging of lacunar infarcts.** *J Comput Assisted Tomogr* 2002;26:628–32
16. Duvernoy HM. *Human Brain Stem Vessels*. 2nd ed. Berlin, Germany: Springer-Verlag; 1999:206–13
17. Ogg R, Langston J, Haacke EM, et al. **The correlation between phase shifts in gradient-echo MR images and regional brain iron concentration.** *Magn Reson Imaging* 1999;17:1141–48
18. Haacke EM, Cheng NY, House MJ, et al. **Imaging iron stores in the brain using magnetic resonance imaging.** *Magn Reson Imaging* 2005;23:1–25
19. Morris CM, Candy JM, Oakley AE, et al. **Histochemical distribution of non-haem iron in the human brain.** *Acta Anat (Basel)* 1992;144:235–57